Chapter 5

Active Mode Locking

For simplicity, we assume, that the laser operates in the transverse fundamental modes and, therefore, we only have to treat the longitudinal modes of the laser similar to a simple plane parallel Fabry-Perot resonator (Figure: 5.1). We consider one polarization of the field only, however, as we will say later for some mode-locked laser polarization dynamics will become important.

The task of mode-locking is to get as many of the longitudinal modes lasing in a phase synchronous fashion, such that the superposition of all modes represents a pulse with a spatial extent much shorter than the cavity. The pulse will then propagate at the group velocity corresponding to the center frequency of the pulse.

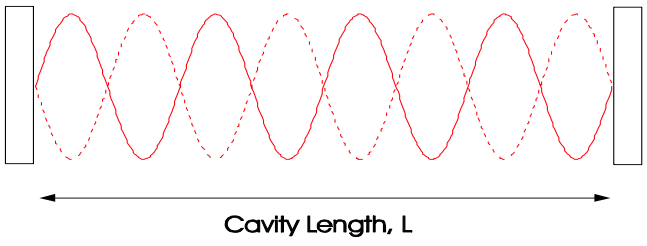

Figure 5.1: Fabry-Perot resonator

5.1 The Master Equation of Mode Locking

Lets consider for the moment the cold cavity (i.e. there is only a simple linear medium in the cavity no lasing). The most general solution for the intracavity field is a superpositon of left- and rightward running waves

$$E^{(left)}(z,t) = Re\left\{\sum_{n=0}^{\infty} \hat{E}_n e^{j(\Omega_n t + K_n z)}\right\}, \tag{5.1}$$

and

$$E^{(right)}(z,t) = Re\left\{\sum_{n=0}^{\infty} \hat{E}_n e^{j(\Omega_n t - K_n z)}\right\}. \tag{5.2}$$

The possible values for the wavenumbers are $K_n = n\pi/L$, resulting from the boundary conditions on metallic mirrors or periodicity after one roundtrip in the cavity. If the mirrors are perfectly reflecting, the leftward and rightward moving waves Eqs.(5.1) and (5.2) contain the same information and it is sufficient to treat only one of them. Usually one of the cavity mirrors is not perfectly reflecting in order to couple out light, however, this can be considered a perturbation to the ideal mode structure.

We consider the modes in Eq.(5.2) as a continuum and replace the sum by an integral

$$E^{(right)}(z,t) = \frac{1}{2\pi} Re\left\{\int_{K=0}^{\infty} \hat{E}(K) e^{j(\Omega(K)t - Kz)} dK\right\} \tag{5.3}$$

with

$$\hat{E}(K_m) = \hat{E}_m 2L. \tag{5.4}$$

Eq.(5.3) is similar to the pulse propagation discussed in chapter 2 and describes the pulse propagation in the resonator. However, here it is rather an initial value problem, rather than a boundary value problem. Note, the wavenumbers of the modes are fixed, not the frequencies. To emphasize this even more, we introduce a new time variable $T = t$ and a local time frame $t' = t - z/v_{g,0}$, instead of the propagation distance z, where $v_{g,0}$ is the group velocity at the central wave number K_{n_0} of the pulse

$$v_{g,0} = \left.\frac{\partial \omega}{\partial k}\right|_{k=0} = \left.\left(\frac{\partial k}{\partial \omega}\right)^{-1}\right|_{\omega=0}. \tag{5.5}$$

For introduction of a slowly varying envelope, we shift the frequency and wavenumber by the center frequency $\omega_0 = \Omega_{n_0}$ and center wave number $k_0 = K_{n_0}$

$$\begin{aligned} k &= K - K_{n_0}, && (5.6)\\ \omega(k) &= \Omega(K_{n_0} + k) - \Omega_{n_0}, && (5.7)\\ \hat{E}(k) &= \hat{E}(K_{n_0} + k), && (5.8) \end{aligned}$$

The temporal evolution of the pulse is than determined by

$$E^{(right)}(z,t) = \frac{1}{2\pi} Re \left\{ \int_{-K_{n_0} \to -\infty}^{\infty} \hat{E}(k) e^{j(\omega(k)t - kz)} dk \right\} e^{j(\omega_0 t - k_0 z)}. \quad (5.9)$$

Analogous to chapter 2, we define a slowly varying field envelope, that is already normalized to the total power flow in the beam

$$A(z,t) = \sqrt{\frac{A_{eff}}{2Z_0}} \frac{1}{2\pi} \int_{-\infty}^{\infty} \hat{E}(k) e^{j(\omega(k)t - kz)} dk. \quad (5.10)$$

With the retarded time t' and time T, we obtain analogous to Eq. (2.184).

$$A(T,t') = \sqrt{\frac{A_{eff}}{2Z_0}} \frac{1}{2\pi} \int_{-\infty}^{\infty} \hat{E}(k) e^{j((\omega(k) - v_{g,0}k)T + k v_{g,0} t'} dk. \quad (5.11)$$

which can be written as

$$T_R \frac{\partial A(T,t')}{\partial T}\bigg|_{(GDD)} = j \sum_{n=2}^{\infty} D_n \left(-j \frac{\partial^n}{\partial t'} \right)^n A(T,t'), \quad (5.12)$$

with the dispersion coefficients per resonator round-trip $T_R = \frac{2L}{v_{g,0}}$

$$D_n = \frac{2L}{n! v_{g,0}^{n+1}} \frac{\partial^{n-1} v_g(k)}{\partial k^{n-1}}\bigg|_{k=0}. \quad (5.13)$$

The dispersion coefficients (5.13) look somewhat suspicious, however, it is not difficult to show, that they are equivalent to derivatives of the roundtrip phase $\phi_R(\Omega) = \frac{\Omega}{c} n(\Omega) 2L$ in the resonator at the center frequency

$$D_n = -\frac{1}{n!} \frac{\partial^n \phi_R^{(n)}(\Omega)}{\partial \Omega^n}\bigg|_{\Omega=\omega_0}, \quad (5.14)$$

Sofar, only the lossless resonator is treated. The gain and loss can be modelled by adding a term like

$$T_R \frac{\partial A(T,t')}{\partial T}\bigg|_{(loss)} = -lA(T,t') \tag{5.15}$$

where l is the amplitude loss per round-trip. In an analogous manner we can write for the gain

$$T_R \frac{\partial A(T,t')}{\partial T}\bigg|_{(gain)} = \left(g(T) + D_g \frac{\partial^2}{\partial t'^2}\right) A(T,t'), \tag{5.16}$$

where $g(T)$ is the gain and and D_g is the curvature of the gain at the maximum of the Lorentzian lineshape.

$$D_g = \frac{g(T)}{\Omega_g^2} \tag{5.17}$$

D_g is the gain dispersion. $g(T)$ is an average gain, which can be computed from the rate equation valid for each unit cell in the resonator. The distributed gain obeys the equation

$$\frac{\partial g(z,t)}{\partial t} = -\frac{g-g_0}{\tau_L} - g\frac{|A(z,t)|^2}{E_L}, \tag{5.18}$$

where E_L is the saturation energy $E_L = \frac{h\nu_L}{2^*\sigma_L} A_{eff}$, τ_L the upper state lifetime and σ_L the gain cross section. For typical solid-state lasers, the intracavity pulse energy is much smaller than the saturation energy. Therefore, the gain changes within one roundtrip are small. Furthermore, we assume that the gain saturates spatially homogeneous, $g(z,t') = g(t')$. Then, the equation for the average gain $g(T)$ can be found by averageing (5.18) over one round-trip and we obtain

$$\frac{\partial g(T)}{\partial T} = -\frac{g-g_0}{\tau_L} - g\frac{W(T)}{E_L T_R}, \tag{5.19}$$

where $W(T)$ is the intracavity pulse energy at time $t = T$

$$W(T) = \int_{t'=-T_R/2}^{T_R/2} |A(T,t')|^2 dt' \approx \int_{-\infty}^{\infty} |A(T,t')|^2 dt'. \tag{5.20}$$

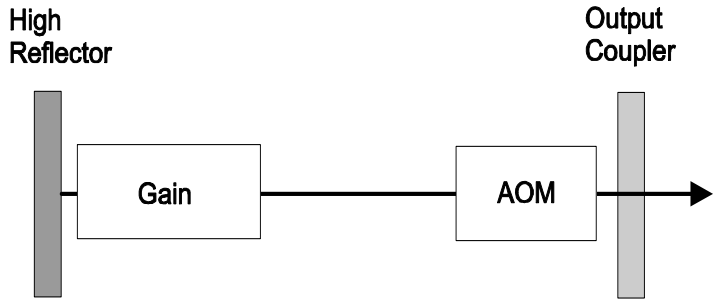

Figure 5.2: Actively modelocked laser with an amplitude modulator (Acousto-Optic-Modulator).

Taking all effects into account, the linear ones: loss, dispersion, gain and gain dispersion, as well as the nonlinear ones like saturable absorption and self-phase modulation, we end up with the master equation of modelocking

$$\begin{aligned} T_R \frac{\partial A(T,t')}{\partial T} &= -lA(T,t') + j\sum_{n=2}^{\infty} D_n \left(j\frac{\partial^n}{\partial t}\right)^n A(T,t') \\ &+ g(T)\left(1+\frac{1}{\Omega_g^2}\frac{\partial^2}{\partial t'^2}\right)A(T,t') \\ &- q(T,t')A(T,t') - j\delta|A(T,t')|^2 A(T,t'). \end{aligned} \tag{5.21}$$

To keep notation simple, we replace t' by t again. This equation was first derived by Haus [4] under the assumption of small changes in pulse shape per round-trip and per element passed within one round-trip.

5.2 Active Mode Locking by Loss Modulation

Active mode locking was first investigated in 1970 by Kuizenga and Siegman using a gaussian pulse analyses, which we want to delegate to the exercises [3]. Later in 1975 Haus [4] introduced the master equation approach (5.21). We follow the approach of Haus, because it also shows the stability of the solution.

We introduce a loss modulator into the cavity, for example an acousto-optic modulator, which periodically varias the intracavity loss according to

Figure 5.3: Schematic representation of the master equation for an actively mode-locked laser.

$q(t) = M\,(1 - \cos(\omega_M t))$. The modulation frequency has to be very precisely tuned to the resonator round-trip time, $\omega_M = 2\pi/T_R$, see Fig.5.2. The modelocking process is then described by the master equation

$$T_R \frac{\partial A}{\partial T} = \left[g(T) + D_g \frac{\partial^2}{\partial t^2} - l - M\,(1 - \cos(\omega_M t)) \right] A. \tag{5.22}$$

neglecting GDD and SPM. The equation can be interpreted as the total pulse shaping due to gain, loss and modulator, see Fig.5.3.

If we fix the gain in Eq. (5.22) at its stationary value, what ever it might be, Eq.(5.22) is a linear p.d.e, which can be solved by separation of variables. The pulses, we expect, will have a width much shorter than the round-trip time T_R. They will be located in the minimum of the loss modulation where the cosine-function can be approximated by a parabola and we obtain

$$T_R \frac{\partial A}{\partial T} = \left[g - l + D_g \frac{\partial^2}{\partial t^2} - M_s t^2 \right] A. \tag{5.23}$$

M_s is the modulation strength, and corresponds to the curvature of the loss modulation in the time domain at the minimum loss point

$$D_g = \frac{g}{\Omega_g^2}, \tag{5.24}$$

$$M_s = \frac{M\omega_M^2}{2}. \tag{5.25}$$

The differential operator on the right side of (5.23) corresponds to the Schrödinger-Operator of the harmonic oscillator problem. Therefore, the eigen functions of this operator are the Hermite-Gaussians

$$A_n(T,t) = A_n(t)e^{\lambda_n T/T_R}, \tag{5.26}$$

$$A_n(t) = \sqrt{\frac{W_n}{2^n\sqrt{\pi}n!\tau_a}}H_n(t/\tau_a)e^{-\frac{t^2}{2\tau_a^2}}, \tag{5.27}$$

where τ_a defines the width of the Gaussian. The width is given by the fourth root of the ratio between gain dispersion and modulator strength

$$\tau_a = \sqrt[4]{D_g/M_s}. \tag{5.28}$$

Note, from Eq. (5.26) we can follow, that the gain per round-trip of each eigenmode is given by λ_n (or in general the real part of λ_n), which are given by

$$\lambda_n = g_n - l - 2M_s\tau_a^2(n+\frac{1}{2}). \tag{5.29}$$

The corresponding saturated gain for each eigen solution is given by

$$g_n = \frac{1}{1+\frac{W_n}{P_L T_R}}, \tag{5.30}$$

where W_n is the energy of the corresponding solution and $P_L = E_L/\tau_L$ the saturation power of the gain. Eq. (5.29) shows that for given g the eigen solution with $n = 0$, the ground mode, has the largest gain per roundtrip. Thus, if there is initially a field distribution which is a superpostion of all eigen solutions, the ground mode will grow fastest and will saturate the gain to a value

$$g_s = l + M_s\tau_a^2. \tag{5.31}$$

such that $\lambda_0 = 0$ and consequently all other modes will decay since $\lambda_n < 0$ for $n \geq 1$. This also proves the stability of the ground mode solution [4]. Thus active modelocking without detuning between resonator round-trip time and modulator period leads to Gaussian steady state pulses with a FWHM pulse width

$$\Delta t_{FWHM} = 2\ln 2\tau_a = 1.66\tau_a. \tag{5.32}$$

The spectrum of the Gaussian pulse is given by

$$\tilde{A}_0(\omega) = \int_{-\infty}^{\infty} A_0(t) e^{i\omega t} dt \tag{5.33}$$

$$= \sqrt{\sqrt{\pi} W_n \tau_a} e^{-\frac{(\omega\tau_a)^2}{2}}, \tag{5.34}$$

and its FWHM is

$$\Delta f_{FWHM} = \frac{1.66}{2\pi\tau_a}. \tag{5.35}$$

Therfore, the time-bandwidth product of the Gaussian is

$$\Delta t_{FWHM} \cdot \Delta f_{FWHM} = 0.44. \tag{5.36}$$

The stationary pulse shape of the modelocked laser is due to the parabolic loss modulation (pulse shortening) in the time domain and the parabolic filtering (pulse stretching) due to the gain in the frequency domain, see Figs. 5.4 and 5.5. The stationary pulse is achieved when both effects balance. Since external modulation is limited to electronic speed and the pulse width does only scale with the inverse square root of the gain bandwidth actively modelocking typically only results in pulse width in the range of 10-100ps.

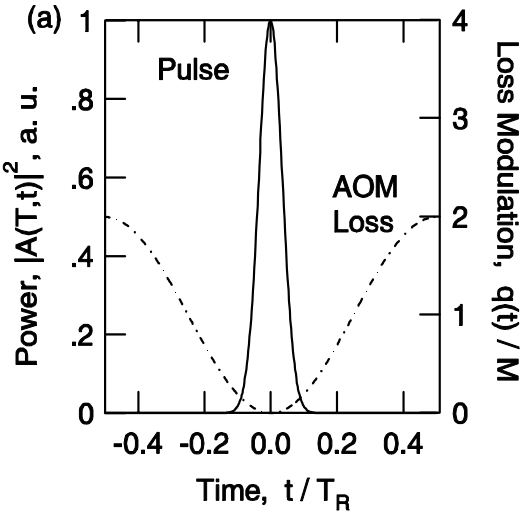

Figure 5.4: (a) Loss modulation gives pulse shortening in each roundtrip

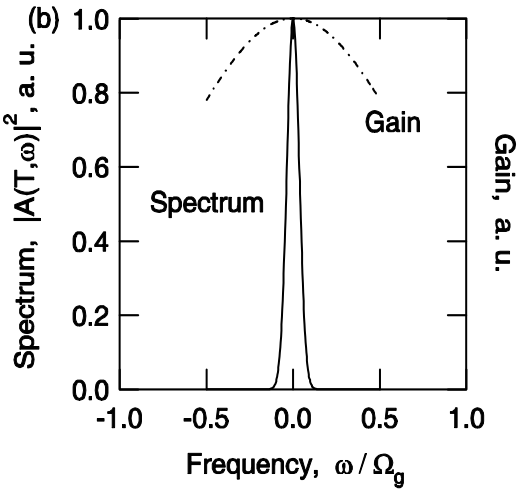

Figure 5.5: (b) the finite gain bandwidth gives pulse broadening in each roundtrip. For a certain pulse width there is balance between the two processes.

For example: Nd:YAG; $2l = 2g = 10\%$, $\Omega_g = \pi\Delta f_{FWHM} = 0.65$ THz, $M = 0.2$, $f_m = 100$ MHz, $D_g = 0.24$ ps^2, $M_s = 4 \cdot 10^{16} s^{-1}$, $\tau_p \approx 99$ ps.

With the pulse width (5.28), Eq.(5.31) can be rewritten in several ways

$$g_s = l + M_s\tau_a^2 = l + \frac{D_g}{\tau_a^2} = l + \frac{1}{2}M_s\tau_a^2 + \frac{1}{2}\frac{D_g}{\tau_a^2}, \tag{5.37}$$

which means that in steady state the saturated gain is lifted above the loss level l, so that many modes in the laser are maintained above threshold. There is additional gain necessary to overcome the loss of the modulator due to the finite temporal width of the pulse and the gain filter due to the finite bandwidth of the pulse. Usually

$$\frac{g_s - l}{l} = \frac{M_s\tau_a^2}{l} \ll 1, \tag{5.38}$$

since the pulses are much shorter than the round-trip time and the stationary pulse energy can therefore be computed from

$$g_s = \frac{1}{1 + \frac{W_s}{P_L T_R}} = l. \tag{5.39}$$

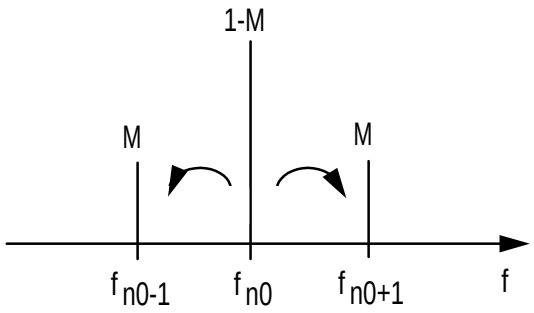

Figure 5.6: Modelocking in the frequency domain: The modulator transvers energy from each mode to its neighboring mode, thereby redistributing energy from the center to the wings of the spectrum. This process seeds and injection locks neighboring modes.

The name modelocking originates from studying this pulse formation process in the frequency domain. Note, the term

$$-M\left[1-\cos(\omega_M t)\right]A$$

does generate sidebands on each cavity mode present according to

$$\begin{aligned} & -M\left[1-\cos(\omega_M t)\right]\exp(j\omega_{n_0}t) \\ = \; & -M\left[\exp(j\omega_{n_0}t)-\frac{1}{2}\exp(j(\omega_{n_0}t-\omega_M t))-\frac{1}{2}\exp(j(\omega_{n_0}t+\omega_M t))\right] \\ = \; & M\left[-\exp(j\omega_{n_0}t)+\frac{1}{2}\exp(j\omega_{n_0-1}t)+\frac{1}{2}\exp(j\omega_{n_0+1}t)\right] \end{aligned}$$

if the modulation frequency is the same as the cavity round-trip frequency. The sidebands generated from each running mode is injected into the neighboring modes which leads to synchronisation and locking of neighboring modes, i.e. mode-locking, see Fig.5.6

5.3 Active Mode-Locking by Phase Modulation

Side bands can also be generated by a phase modulator instead of an amplitude modulator. However, the generated sidebands are out of phase with

the carrier, which leads to a chirp on the steady state pulse. We can again use the master equation to study this type of modelocking. All that changes is that the modulation becomes imaginary, i.e. we have to replace M by jM in Eq.(5.22)

$$T_R \frac{\partial A}{\partial T} = \left[g(T) + D_g \frac{\partial^2}{\partial t^2} - l - jM\left(1 - \cos(\omega_M t)\right) \right] A. \tag{5.40}$$

The imaginary unit can be pulled through much of the calculation and we arrive at the same Hermite Gaussian eigen solutions (5.26,5.27), however, the parameter τ_a becomes τ_a' and is now complex and not quite the pulse width

$$\tau_a' = \sqrt[4]{-j}\sqrt[4]{D_g/M_s}. \tag{5.41}$$

The ground mode or stationary solution is given by

$$A_0(t) = \sqrt{\frac{W_s}{2^n\sqrt{\pi}n!\tau_a'}} e^{-\frac{t^2}{2\tau_a^2}\frac{1}{\sqrt{2}}(1+j)}, \tag{5.42}$$

with $\tau_a = \sqrt[4]{D_g/M_s}$ as before. We end up with chirped pulses. How does the pulse shortening actually work, because the modulator just puts a chirp on the pulse, it does actually not shorten it? One can easily show, that if a Gaussian pulse with chirp parameter β

$$A_0(t) \sim e^{-\frac{t^2}{2\tau_a^2}\frac{1}{\sqrt{2}}(1+j\beta)}, \tag{5.43}$$

has a chirp $\beta > 1$, subsequent filtering is actually shortening the pulse.

5.4 Active Mode Locking with Additional SPM

Due to the strong focussing of the pulse in the gain medium also additional self-phase modulation can become important. Lets consider the case of an actively mode-locked laser with additional SPM, see Fig. 5.7. One can write down the corresponding master equation

$$T_R \frac{\partial A}{\partial T} = \left[g(T) + D_g \frac{\partial^2}{\partial t^2} - l - M_s t^2 - j\delta|A|^2 \right] A. \tag{5.44}$$

Unfortunately, there is no analytic solution to this equation. But it is not difficult to guess what will happen in this case. As long as the SPM is not

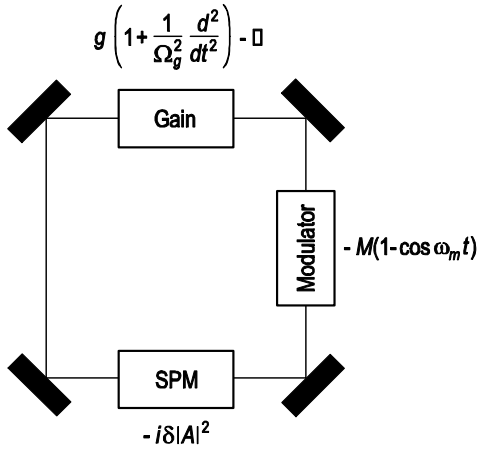

Figure 5.7: Active mode-locking with SPM

excessive, the pulses will experience additional self-phase modulation, which creates a chirp on the pulse. Thus one can make an ansatz with a chirped Gaussian similar to (5.43) for the steady state solution of the master equation (5.44)

$$A_0(t) = Ae^{-\frac{t^2}{2\tau_a^2}(1+j\beta)+j\Psi T/T_R} \tag{5.45}$$

Note, we allow for an additional phase shift per roundtrip Ψ, because the added SPM does not leave the phase invariant after one round-trip. This is still a steady state solution for the intensity envelope. Substitution into the master equation using the intermediate result

$$\frac{\partial^2}{\partial t^2}A_0(t) = \left\{\frac{t^2}{\tau_a^4}\left(1+j\beta\right)^2 - \frac{1}{\tau_a^2}\left(1+j\beta\right)\right\}A_0(t). \tag{5.46}$$

leads to

$$\begin{aligned} j\Psi A_0(t) &= \left\{g - l + D_g\left[\frac{t^2}{\tau_a^4}\left(1+j\beta\right)^2 - \frac{1}{\tau_a^2}\left(1+j\beta\right)\right]\right. \\ &\quad \left. -M_s t^2 - j\delta\left|A\right|^2 e^{-\frac{t^2}{\tau_a^2}}\right\}A_0(t). \end{aligned} \tag{5.47}$$

To find an approximate solution we expand the Gaussian in the bracket, which is a consequency of the SPM to first order in the exponent.

$$j\Psi = g - l + D_g \left[\frac{t^2}{\tau_a^4} (1 + j\beta)^2 - \frac{1}{\tau_a^2} (1 + j\beta) \right] - M_s t^2 - j\delta |A|^2 \left(1 - \frac{t^2}{\tau_a^2} \right). \tag{5.48}$$

This has to be fulfilled for all times, so we can compare coefficients in front of the constant terms and the quadratic terms, which leads to two complex conditions. This leads to four equations for the unknown pulsewidth τ_a, chirp β, round-trip phase Ψ and the necessary excess gain $g - l$. With the nonlinear peak phase shift due to SPM, $\phi_0 = \delta |A|^2$. Real and Imaginary parts of the quadratic terms lead to

$$0 = \frac{D_g}{\tau_a^4} \left(1 - \beta^2 \right) - M_s, \tag{5.49}$$

$$0 = 2\beta \frac{D_g}{\tau_a^4} + \frac{\phi_0}{\tau_a^2}, \tag{5.50}$$

and the constant terms give the excess gain and the additional round-trip phase.

$$g - l = \frac{D_g}{\tau_a^2}, \tag{5.51}$$

$$\Psi = D_g \left[-\frac{1}{\tau_a^2} \beta \right] - \phi_0. \tag{5.52}$$

The first two equations directly give the chirp and pulse width.

$$\beta = -\frac{\phi_0 \tau_a^2}{2 D_g} \tag{5.53}$$

$$\tau_a^4 = \frac{D_g}{M_s + \frac{\phi_0^2}{4 D_g}}. \tag{5.54}$$

However, one has to note, that this simple analysis does not give any hint on the stability of these approximate solution. Indeed computer simulations show, that after an additional pulse shorting of about a factor of 2 by SPM beyond the pulse width already achieved by pure active mode-locking on its own, the SPM drives the pulses unstable [5]. This is one of the reasons, why very broadband laser media, like Ti:sapphire, can not simply generate

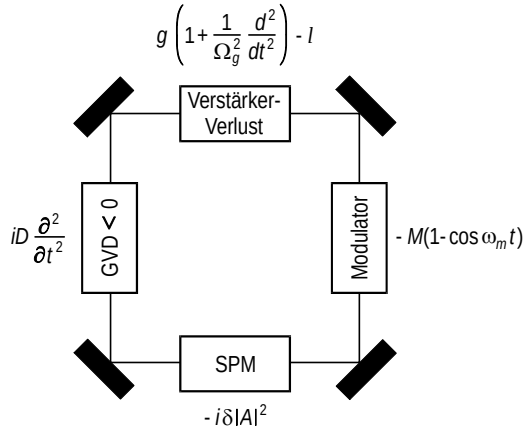

Figure 5.8: Acitve mode-locking with additional soliton formation

femtosecond pulses via active modelocking. The SPM occuring in the gain medium for very short pulses drives the modelocking unstable. Additional stabilization measures have to be adopted. For example the addition of negative group delay dispersion might lead to stable soliton formation in the presence of the active modelocker.

5.5 Active Mode Locking with Soliton Formation

Experimental results with fiber lasers [8, 9, 11] and solid state lasers [10] indicated that soliton shaping in the negative GDD regime leads to pulse stabilization and considerable pulse shorting. With sufficient negative dispersion and self-phase modulation in the system and picosecond or even femtosecond pulses, it is possible that the pulse shaping due to GDD and SPM is much stronger than due to modulation and gain filtering, see Fig. 5.8. The resulting master equation for this case is

$$T_R\frac{\partial A}{\partial T}=\left[g+\left(D_g-j\left|D\right|\right)\frac{\partial^2}{\partial t^2}-l-M\left(1-\cos(\omega_M t)\right)-j\delta|A|^2\right]A. \quad (5.55)$$

For the case, that soliton formation takes over, the steady state solution a soliton plus a continuum contribution

$$A(T,t) = \left(a(x)e^{jpt} + a_c(T,t)\right) e^{-j\theta} \tag{5.56}$$

with

$$a(x) = A\,\mathrm{sech}(x), \quad \text{and} \quad x = \frac{1}{\tau}(t + 2D\int_0^T p(T')dT' - t_0) \tag{5.57}$$

where a_c is the continuum contribution. The phase is determined by

$$\theta(T) = \theta_0(T) - \frac{D}{T_R}\int_0^T \left(\frac{1}{\tau(T')^2} - p(T')^2\right) dT', \tag{5.58}$$

whereby we always assume that the relation between the soliton energy and soliton width is maintained (3.9)

$$\frac{|D|}{\tau(T)^2} = \frac{\delta A(T)^2}{2}. \tag{5.59}$$

We also allow for a continuous change in the soliton amplitude A or energy $W = 2A^2\tau$ and the soliton variables phase θ_0, carrier frequency p and timing t_0. ϕ_0 is the soliton phase shift per roundtrip

$$\phi_0 = \frac{|D|}{\tau^2}. \tag{5.60}$$

However, we assume that the changes in carrier frequency, timing and phase stay small. Introducing (5.56) into (5.55) we obtain according to the soliton perturbation theory developed in chapter 3.5

$$\begin{aligned} & T_R\left[\frac{\partial a_c}{\partial T} + \frac{\partial W}{\partial T}\mathbf{f}_w + \frac{\partial \Delta\theta}{\partial T}\mathbf{f}_\theta + \frac{\partial \Delta p}{\partial T}\mathbf{f}_p + \frac{\partial \Delta t}{\partial T}\mathbf{f}_t\right] \\ = \;& \phi_0\mathbf{L}\left(\mathbf{a}_c + \Delta p\mathbf{f}_p\right) + \mathbf{R}(\mathbf{a} + \Delta p\mathbf{f}_p + \mathbf{a}_c) \\ & -M\omega_M \sin(\omega_M\tau x)\Delta t\,\mathbf{a}(x) \end{aligned} \tag{5.61}$$

The last term arises because the active modelocker breaks the time invariance of the system and leads to a restoring force pushing the soliton back to its equilibrium position. $\mathbf{L}$, $\mathbf{R}$ are the operators of the linearized NSE and of the active mode locking scheme, respectively

$$\mathbf{R} = g\left(1 + \frac{1}{\Omega_g^2\tau^2}\frac{\partial^2}{\partial x^2}\right) - l - M\left(1 - \cos(\omega_M\tau x)\right), \tag{5.62}$$

The vectors $\mathbf{f}_w, \mathbf{f}_\theta, \mathbf{f}_p$ and $\mathbf{f}_t$ describe the change in the soliton when the soliton energy, phase, carrier frequency and timing varies.

5.5.1 Stability Condition

We want to show, that a stable soliton can exist in the presence of the modelocker and gain dispersion if the ratio between the negative GDD and gain dispersion is sufficiently large. From (5.61) we obtain the equations of motion for the soliton parameters and the continuum by carrying out the scalar product with the corresponding adjoint functions. Specifically, for the soliton energy we get

$$\begin{aligned} T_R \frac{\partial W}{\partial T} &= 2\left(g - l - \frac{g}{3\Omega_g^2\tau^2} - \frac{\pi^2}{24} M\omega_M^2\tau^2\right) W \\ &+ < \mathbf{f}_w^{(+)} | \mathbf{R}\mathbf{a}_c > . \end{aligned} \tag{5.63}$$

We see that gain saturation does not lead to a coupling between the soliton and the continuum to first order in the perturbation, because they are orthogonal to each other in the sense of the scalar product (3.36). This also means that to first order the total field energy is contained in the soliton.

Thus to zero order the stationary soliton energy $W_0 = 2A_0^2\tau$ is determined by the condition that the saturated gain is equal to the total loss due to the linear loss l, gain filtering and modulator loss

$$g - l = \frac{\pi^2}{24} M\omega_M^2\tau^2 + \frac{g}{3\Omega_g^2\tau^2} \tag{5.64}$$

with the saturated gain

$$g = \frac{g_0}{1 + W_0/E_L}. \tag{5.65}$$

Linearization around this stationary value gives for the soliton perturbations

$$
\begin{aligned}
T_R\frac{\partial\Delta W}{\partial T} &= 2\Bigg(-\frac{g}{(1+W_0/E_L)}\left(\frac{W_0}{E_L}+\frac{1}{3\Omega_g^2\tau^2}\right)\\
&+ \frac{\pi^2}{12}M\omega_M^2\tau^2\Bigg)\Delta W+<\mathbf{f}_w^{(+)}|\mathbf{Ra}_c> \qquad (5.66)\\
T_R\frac{\partial\Delta\theta}{\partial T} &= <\mathbf{f}_\theta^{(+)}|\mathbf{Ra}_c> \qquad (5.67)\\
T_R\frac{\partial\Delta p}{\partial T} &= -\frac{4g}{3\Omega_g^2\tau^2}\Delta p+<\mathbf{f}_p^{(+)}|\mathbf{Ra}_c> \qquad (5.68)\\
T_R\frac{\partial\Delta t}{\partial T} &= -\frac{\pi^2}{6}M\omega_M^2\tau^2\Delta t+2|D|\Delta p\\
&+<\mathbf{f}_t^{(+)}|\mathbf{Ra}_c> \qquad (5.69)
\end{aligned}
$$

and for the continuum we obtain

$$
\begin{aligned}
T_R\frac{\partial g(k)}{\partial T} &= j\Phi_0(k^2+1)g(k)+<\mathbf{f}_k^{(+)}|\mathbf{Ra}_c>\\
&+<\mathbf{f}_k^{(+)}|\mathbf{R}\,(\mathbf{a}_0(x)+\Delta w\,\mathbf{f}_w+\Delta p\,\mathbf{f}_p)>\\
&-<\mathbf{f}_k^{(+)}|M\omega_M\sin(\omega_M\tau x)\mathbf{a}_0(x)>.\Delta t \qquad (5.70)
\end{aligned}
$$

Thus the action of the active modelocker and gain dispersion has several effects. First, the modelocker leads to a restoring force in the timing of the soliton (5.69). Second, the gain dispersion and the active modelocker lead to coupling between the perturbed soliton and the continuum which results in a steady excitation of the continuum.

However, as we will see later, the pulse width of the soliton, which can be stabilized by the modelocker, is not too far from the Gaussian pulse width by only active mode locking. Then relation

$$\omega_M\tau \ll 1 \ll \Omega_g\tau \qquad (5.71)$$

is fulfilled. The weak gain dispersion and the weak active modelocker only couples the soliton to the continuum, but to first order the continuum does not couple back to the soliton. Neglecting higher order terms in the matrix elements of eq.(5.70) [6] results in a decoupling of the soliton perturbations from the continuum in (5.66) to (5.70). For a laser far above threshold, i.e.

$W_0/E_L >> 1$, gain saturation always stabilizes the amplitude perturbation and eqs.(5.67) to (5.69) indicate for phase, frequency and timing fluctuations. This is in contrast to the situation in a soliton storage ring where the laser amplifier compensating for the loss in the ring is below threshold [14].

By inverse Fourier transformation of (5.70) and weak coupling, we obtain for the associated function of the continuum

$$\begin{aligned} T_R\frac{\partial G}{\partial T} = &\left[g - l + j\Phi_0 + \frac{g}{\Omega_g^2}(1 - jD_n)\frac{\partial^2}{\partial t^2}\right. \\ &\left. -M\left(1 - \cos(\omega_M t)\right)\right]G + \mathcal{F}^{-1}\Big\{ < \mathbf{f}_k^{(+)}|\mathbf{R}\mathbf{a}_0(x) > \\ &- < \mathbf{f}_k^{(+)}|M\omega_M \sin(\omega_M \tau x)\mathbf{a}_0(x) > \Delta t\Big\} \end{aligned} \tag{5.72}$$

where D_n is the dispersion normalized to the gain dispersion

$$D_n = |D|\Omega_g^2/g. \tag{5.73}$$

Note, that the homogeneous part of the equation of motion for the continuum, which governs the decay of the continuum, is the same as the homogeneous part of the equation for the noise in a soliton storage ring at the position where no soliton or bit is present [14]. Thus the decay of the continuum is not affected by the nonlinearity, but there is a continuous excitation of the continuum by the soliton when the perturbing elements are passed by the soliton. Thus under the above approximations the question of stability of the soliton solution is completely governed by the stability of the continuum (5.72). As we can see from (5.72) the evolution of the continuum obeys the active mode locking equation with GVD but with a value for the gain determined by (5.64). In the parabolic approximation of the cosine, we obtain again the Hermite Gaussians as the eigensolutions for the evolution operator but the width of these eigensolutions is now given by

$$\tau_c = \tau_a \sqrt[4]{(1 - jD_n)} \tag{5.74}$$

and the associated eigenvalues are

$$\lambda_m = j\Phi_0 + g - l - M\omega_M^2\tau_a^2\sqrt{(1 - jD_n)}(m + \frac{1}{2}). \tag{5.75}$$

The gain is clamped to the steady state value given by condition (5.64) and we obtain

$$\begin{aligned}\lambda_m &= +j\Phi_0 + \frac{1}{3}\sqrt{D_g M_s}\Bigg[\left(\frac{\tau_a}{\tau}\right)^2 + \frac{\pi^2}{4}\left(\frac{\tau_a}{\tau}\right)^{-2} \\ &\quad -6\sqrt{(1-jD_n)}(m+\frac{1}{2})\Bigg].\end{aligned} \tag{5.76}$$

Stability is achieved when all continuum modes see a net loss per roundtrip, $Re\{\lambda_m\} < 0$ for $m \geq 0$, i.e. we get from (5.76)

$$\left(\frac{\tau_a}{\tau}\right)^2 + \frac{\pi^2}{4}\left(\frac{\tau}{\tau_a}\right)^2 < 3Re\{\sqrt{(1-jD_n)}\}. \tag{5.77}$$

Relation (5.77) establishes a quadratic inequality for the pulse width reduction ratio $\xi = (\tau_a/\tau)^2$, which is a measure for the pulse width reduction due to soliton formation

$$\xi^2 - 3Re\{\sqrt{(1-jD_n)}\}\xi + \frac{\pi^2}{4} < 0. \tag{5.78}$$

As has to be expected, this inequality can only be satisfied if we have a minimum amount of negative normalized dispersion so that a soliton can be formed at all

$$D_{n,crit} = 0.652. \tag{5.79}$$

Therefore our perturbation ansatz gives only meaningful results beyond this critical amount of negative dispersion. Since ξ compares the width of a Gaussian with that of a secant hyperbolic it is more relevant to compare the full width half maximum of the intensity profiles [**?**] of the corresponding pulses which is given by

$$R = \frac{1.66}{1.76}\sqrt{\xi}. \tag{5.80}$$

Image removed due to copyright restrictions.

Please see:
Kaertner, F., D. Kopf, and U. Keller. "Solitary-pulse stabilization and shortening in actively mode-locked lasers." *Journal of the Optical Society of America B* 12, no. 3 (March 1995): 486.

Figure 5.9: Pulsewidth reduction as a function of normalized dispersion. Below $D_{n,crit} = 0.652$ no stable soliton can be formed.

Figure 5.9 shows the maximum pulse width reduction R allowed by the stability criterion (5.78) as a function of the normalized dispersion. The critical value for the pulse width reduction is $R_{crit} \approx 1.2$. For large normalized dispersion Fig. 1 shows that the soliton can be kept stable at a pulse width reduced by up to a factor of 5 when the normalized dispersion can reach a value of 200. Even at a moderate negative dispersion of $D_n = 5$, we can achieve a pulsewidth reduction by a factor of 2. For large normalized dispersion the stability criterion (5.78) approaches asymptotically the behavior

$$\xi < \sqrt{\frac{9D_n}{2}} \quad \text{or} \quad R < \frac{1.66}{1.76}\sqrt[4]{\frac{9D_n}{2}}. \tag{5.81}$$

Thus, the possible pulse-width reduction scales with the fourth root of the normalized dispersion indicating the need of an excessive amount of dispersion necessary to maintain a stable soliton while suppressing the continuum. The physical reason for this is that gain filtering and the active modelocker continuously shed energy from the soliton into the continuum. For the soliton the action of GVD and SPM is always in balance and maintains the pulse shape. However, as can be seen from (5.72), the continuum, which can be viewed as a weak background pulse, does not experience SPM once it is generated and therefore gets spread by GVD. This is also the reason why the eigenstates of the continuum consist of long chirped pulses that scale

also with the fourth root of the dispersion (5.74). Then, the long continuum pulses suffer a much higher loss in the active modulator in contrast to the short soliton which suffers reduced gain when passing the gain medium due to its broader spectrum. The soliton is stable as long as the continuum sees less roundtrip gain than the soliton.

In principle by introducing a large amount of negative dispersion the theory would predict arbitrarily short pulses. However, the master equation (5.55) only describes the laser system properly when the nonlinear changes of the pulse per pass are small. This gives an upper limit to the nonlinear phase shift Φ_0 that the soliton can undergo during one roundtrip. A conservative estimation of this upper limit is given with $\Phi_0 = 0.1$. Then the action of the individual operators in (5.55) can still be considered as continuous. Even if one considers larger values for the maximum phase shift allowed, since in fiber lasers the action of GVD and SPM occurs simultaneously and therefore eq.(5.55) may describe the laser properly even for large nonlinear phase shifts per roundtrip, one will run into intrinsic soliton and sideband instabilities for Φ_0 approaching 2π [30, 31]. Under the condition of a limited phase shift per roundtrip we obtain

$$\tau^2 = \frac{|D|}{\Phi_0}. \tag{5.82}$$

Thus from (5.32), the definition of ξ, (5.81) and (5.82) we obtain for the maximum possible reduction in pulsewidth

$$R_{max} = \frac{1.66}{1.76} \sqrt[12]{\frac{(9\Phi_0/2)^2}{D_g\, M_s}} \tag{5.83}$$

and therefore for the minimum pulsewidth

$$\tau_{min} = \sqrt[6]{\frac{2D_g^2}{9\Phi_0\, M_s}}. \tag{5.84}$$

The necessary amount of normalized negative GVD is then given by

$$D_n = \frac{2}{9} \sqrt[3]{\frac{(9\Phi_0/2)^2}{D_g\, M_s}}. \tag{5.85}$$

Eqs.(5.83) to (5.85) constitute the main results of this paper, because they allow us to compute the possible pulse width reduction and the necessary

Table 5.1: Maximum pulsewidth reduction and necessary normalized GVD for different laser systems. In all cases we used for the saturated gain $g = 0.1$ and the soliton phase shift per roundtrip $\Phi_0 = 0.1$. For the broadband gain materials the last column indicates rather long transient times which calls for regenerative mode locking.

negative GVD for a given laser system. Table (5.1) shows the evaluation of these formulas for several gain media and typical laser parameters.

Table 5.1 shows that soliton formation in actively mode-locked lasers may lead to considerable pulse shortening, up to a factor of 10 in Ti:sapphire. Due to the 12th root in (5.83) the shortening depends mostly on the bandwidth of the gain material which can change by several orders of magnitude for the different laser materials. The amount of negative dispersion for achieving this additional pulse shortening is in a range which can be achieved by gratings, Gires-Tournois interferometers, or prisms.

Of course, in the experiment one has to stay away from these limits to suppress the continuum sufficiently. However, as numerical simulations show, the transition from stable to instable behaviour is remarkably sharp. The reason for this can be understood from the structure of the eigenvalues for the continuum (5.76). The time scale for the decay of transients is given by the inverse of the real part of the fundamental continuum mode which diverges at the transition to instability. Nevertheless, a good estimate for this transient time is given by the leading term of the real part of (5.76)

$$\frac{\tau_{trans}}{T_R} = \frac{1}{Re\{\lambda_0\}} \approx \frac{3}{\sqrt{D_g M_s} R^2} \tag{5.86}$$

This transient time is also shown in Table (5.1) for different laser systems. Thus these transients decay, if not too close to the instability border, on time scales from approximately 1,000 up to some 100,000 roundtrips, depending strongly on the gain bandwidth and modulation strength. Consequently, to first order the eigenvalues of the continuum modes, which are excited by the right hand side of (5.72), are purely imaginary and independent of the mode number, i.e. $\lambda_n \approx j\Phi_0$. Therefore, as long as the continuum is stable, the solution to (5.72) is given by

$$\begin{aligned} G(x) &= \frac{-j}{\Phi_0}\mathcal{F}^{-1}\Big\{ < \mathbf{f}_k^{(+)} | \mathbf{R}\mathbf{a}_0(x) > \\ &- M_s\tau^2 < \mathbf{f}_k^{(+)} | x\mathbf{a}_0(x) > \frac{\Delta t}{\tau}\Big\}. \end{aligned} \tag{5.87}$$

Thus, in steady state the continuum is on the order of

$$|G(x)| \approx \frac{A_0}{\Phi_0}\frac{D_g}{\tau^2} = \frac{A_0}{D_n}. \tag{5.88}$$

which demonstrates again the spreading of the continuum by the dispersion. Equation (5.88) shows that the nonlinear phase shift of the solitary pulse per round trip has to be chosen as large as possible. This also maximizes the normalized dispersion, so that the radiation shed from the soliton into the continuum changes the phase rapidly enough such that the continuum in steady state stays small. Note that the size of the generated continuum according to (5.88) is rather independent of the real part of the lowest eigenvalue of the continuum mode. Therefore, the border to instability is very sharply defined. However, the time scale of the transients at the transition to instability can become arbitrarily long. Therefore, numerical simulations are only trustworthy if the time scales for transients in the system are known from theoretical considerations as those derived above in (5.86). The simulation time for a given laser should be at least of the order of 10 times τ_{trans} or even longer, if operated close to the instability point, as we will see in the next section.

5.5.2 Numerical simulations

Table 5.1 shows that soliton formation in actively mode-locked lasers may lead to considerable pulse shortening, up to a factor of 10 in Ti:sapphire. We want to illustrate that at the example of a Nd:YAG laser, which is chosen due to its moderate gain bandwidth, and therefore, its large gain dispersion. This will limit the pulsewidth reduction possible to about 3, but the decay time of the continuum (5.86) (see also Table 5.1) is then in a range of 700 roundtrips so that the steady state of the mode-locked laser can be reached with moderate computer time, while the approximations involved are still satisfied. The system parameters used for the simulation are shown in table 5.2. For the simulation of eq.(5.55) we use the standard split-step Fourier transform method. Here the discrete action of SPM and GDD per roundtrip is included by choosing the integration step size for the T integration to be the roundtrip time T_R. We used a discretisation of 1024 points over the bandwidth of $1THz$, which corresponds to a resolution in the time domain of $1ps$. The following figures, show only one tenth of the simulated window in time and frequency.

Figure 5.10 shows the result of the simulation starting with a 68-ps-long Gaussian pulse with a pulse energy of $W = 40$ nJ for $D_n = 24$, i.e. D = -17 ps^2. For the given SPM coefficient this should lead to stable pulse shortening by a factor of $R = 2.8$. Thus after at least a few thousand roundtrips the

parameter	value
l	0.1
g_0	1
P_L	$1W$
Ω_g	$2\pi \cdot 60GHz$
ω_M	$2\pi \cdot 0.25GHz$
T_R	$4ns$
M	0.2
δ	$1.4 \cdot 10^{-4}W^{-1}$
D	$-17ps^2$ / $-10ps^2$

Table 5.2: Parameters used for numerical simulations

Image removed due to copyright restrictions.

Please see:
Kaertner, F., D. Kopf, and U. Keller. "Solitary-pulse stabilization and shortening in actively mode-locked lasers." *Journal of the Optical Society of America B* 12, no. 3 (March 1995): 486.

Figure 5.10: Time evolution of the pulse intensity in a Nd:YAG laser for the parameters in Table 5.2, $D = -17ps^2$, for the first 1,000 roundtrips in the laser cavity, starting with a 68ps long Gaussian pulse.

laser should be in steady state again with a FWHM pulsewidth of 24 ps. Fig. 5.10 shows the pulse evolution over the first thousand round-trips, i.e. 4μs real time. The long Gaussian pulse at the start contains an appreciable amount of continuum. The continuum part of the solution does not experience the nonlinear phase shift due to SPM in contrast to the soliton. Thus the soliton interferes with the continuum periodically with the soliton period of $T_{soliton}/T_R = 2\pi/\phi_0 = 20\pi$. This is the reason for the oscillations of the pulse amplitude seen in Fig. 5.10 which vanish with the decay of the continuum. Note also that the solitary pulse is rapidly formed, due to the large nonlinear phase shift per roundtrip. Figure 5.11 shows the simulation in time and frequency domain over 10,000 roundtrips. The laser reaches steady state after about 4,000 roundtrips which corresponds to $6 \times \tau_{trans}$ and the final pulsewidth is 24 ps in exact agreement with the predictions of the analytic formulas derived above.

Lower normalized dispersion of $D_n = 15$ or D = -10 ps^2 only allows for a reduction in pulsewidth by $R = 2.68$. However, using the same amount of SPM as before we leave the range of stable soliton generation.

Image removed due to copyright restrictions.

Please see:
Kaertner, F., D. Kopf, and U. Keller. "Solitary-pulse stabilization and shortening in actively mode-locked lasers." *Journal of the Optical Society of America B* 12, no. 3 (March 1995): 486.

Figure 5.11: Time evolution of the intensity (a) and spectrum (b) for the same parameters as Fig. 2 over 10,000 roundtrips. The laser reaches steady state after about 4,000 rountrips.

Figure 5.12: (a) Time evolution of the intensity in a Nd:YAG laser for the parameters in Table 5.2 over the first 1,000 round-trips. The amount of negative dispersion is reduced to $D = -10ps^2$, starting again from a 68ps long pulse. The continuum in this case does not decay as in Fig. 5.2 and 5.3 due to the insufficient dispersion. (b) Same simulation over 50,000 round-trips.

Figure 5.12(a) shows similar to Fig. 5.10 the first 1,000 roundtrips in that case. Again the solitary pulse is rapidly formed out of the long Gaussian initial pulse. But in contrast to the situation in Fig. 5.10, the continuum does not any longer decay on this time scale. The dispersion is too low to spread the continuum rapidly enough. The continuum then accumulates over many roundtrips as can be seen from Fig. 5.12(b). After about 10,000 roundtrips the continuum has grown so much that it extracts an appreciable amount of energy from the soliton. But surprisingly the continuum modes stop growing after about 30,000 roundtrips and a new quasi stationary state is reached.

5.5.3 Experimental Verification

The theory above explains very well the ps Ti:saphire experiments [10] in the regime where the pulses are stabilized by the active modelocker alone. Gires-Tournois interferometers were used to obtain large amounts of negative GDD to operate the laser in the stable soliton regime derived above. Here we want to discuss in more detail the experimental results obtained recently with a regeneratively, actively mode-locked Nd:glass laser [7], resulting in 310 fs. If SPM and GVD could be neglected, the weak modelocker would produce Gaussian pulses with a FWHM of $\tau_{a,FWHM} = 10$ ps. However, the strong SPM prevents stable pulse formation. The negative dispersion available in the experiment is too low to achieve stable soliton formation, because the pulse width of the soliton at this power level is given by $\tau = 4|D|/(\delta W) =$ 464 fs, for the example discussed. The normalized dispersion is not large enough to allow for such a large pulse width reduction. Providing enough negative dispersion results in a 310 fs perfectly sech-shaped soliton-like pulse as shown in Fig. 5.13. A numerical simulation of this case would need millions of roundtrips through the cavity until a stationary state is reached. That means milliseconds of real time, but would necessitate days of computer time. Also the transition to instable behaviour has been observed, which is the characteristic occurence of a short solitary fs-pulse together with a long ps-pulse due to the instable continuum as we have found in the numerical simulation for the case of a Nd:YAG laser (see Fig. 5.12(b)). Figure 5.14 shows the signal of a fast detector diode on the sampling oscilloscope. The detector has an overall bandwidth of $25GHz$ and therefore can not resolve the fs-pulse, but can resolve the width of the following roughly $100ps$ long pulse.

Image removed due to copyright restrictions.

Please see:

Kaertner, F., D. Kopf, and U. Keller. "Solitary-pulse stabilization and shortening in actively mode-locked lasers." *Journal of the Optical Society of America B* 12, no. 3 (March 1995): 486.

Figure 5.13: Autocorrelation of the actively mode-locked pulse (solid line) and corresponding $sech^2$ fit (dashed line) with additional soliton formation.

Image removed due to copyright restrictions.

Please see:

Kaertner, F., D. Kopf, and U. Keller. "Solitary-pulse stabilization and shortening in actively mode-locked lasers." *Journal of the Optical Society of America B* 12, no. 3 (March 1995): 486.

Figure 5.14: Sampling signal of fast detector when the mode-locked laser operates at the transition to instability. The short fs pulse can not be resolved by the detector and therefore results in a sharp spike corresponding to the detector response time. In advance of the fs-pulse travels a roughly $100ps$ long pulse.

5.6 Summary

The main result of this section is, that pure active mode-locking with an amplitude modulator leads to Gaussian pulses. The width is inverse proportional to the square root of the gain bandwdith. A phase modulator leads to chirped Gaussian pulses. A soliton much shorter than the Gaussian pulse due to pure active mode locking can be stabilized by an active modelocker. This finding also has an important consequence for passive mode locking. It implies that a slow saturable absorber, i.e. an absorber with a recovery time much longer than the width of the soliton, is enough to stabilize the pulse, i.e. to modelock the laser.

Bibliography

[1] H. A. Haus, "Short Pulse Generation", in Compact Sources of Ultrashort Pulses, ed. by I. N. Duling III, Cambridge University Press (1995).

[2] D. J. Kuizenga and A. E. Siegman, "FM and AM Mode Locking of the Homogeneous Laser - Part I: Theory," IEEE J. of Quantum Electron. **QE-6**, pp. 694 – 708 (1970).

[3] D. J. Kuizenga and A. E. Siegman, "FM and AM modelocking of the homogeneous laser - part I: theory," IEEE J. Qunat. Electron. **6**, pp. 694 – 701 (1970).

[4] H. A. Haus, "A Theory of Forced Mode Locking", IEEE Journal of Quantum Electronics **QE-11**, pp. 323 - 330 (1975).

[5] H. A. Haus and Y. Silberberg, "Laser modelocking with addition of nonlinear index", IEEE Journal of Quantum Electronics**QE-22**, pp. 325 - 331 (1986).

[6] F. X. Kärtner, D. Kopf, U. Keller, "Solitary pulse stabilization and shortening in actively mode-locked lasers," J. Opt. Soc. of Am. B**12**, pp. 486 – 496 (1995).

[7] D. Kopf, F. X. Kärtner, K. J. Weingarten, U. Keller, "Pulse shortening in a Nd:glass laser by gain reshaping and soliton formation, Opt. Lett. **19**, 2146 – 2248 (1994).

[8] J.D. Kafka and T. Baer, "Mode-locked erbium-doped fiber laser with soliton pulse shaping", Opt. Lett.**14**, pp. 1269 – 1271 (1989).

[9] K. Smith, R. P. Davey, B. P. Nelson and E.J. Greer, "Fiber and Solid-State Lasers", (Digest No. 120), London, UK, 19 May 1992, P.1/1-4.

[10] J.D. Kafka, M. L. Watts and J.W.J. Pieterse, "Picosecond and femtosecond pulse generation in a regeneratively mode-locked Ti:Sapphire laser",IEEE J. Quantum Electron. **QE-28**, pp. 2151 – 2162 (1992).

[11] F. Fontana, N. Ridi, M. Romagnoli, P. Franco, "Fully integrated 30 ps modelocked fiber laser electronically tunable over 1530 - 1560 nm", Opt. Comm. **107**, pp. 240 – 244 (1994).

[12] D. J. Jones, H. A. Haus and E. P. Ippen, "Solitons in an Actively Modelocked Fiber Laser," to appear in Opt. Lett.

[13] U. Keller, T. H. Chiu and J. F. Ferguson, "Self-starting femtosecond mode-locked Nd:glass laser using intracavity saturable absorber,"- Opt. Lett. **18**, pp. 1077 - 1079 (1993).

[14] H. A. Haus and A. Mecozzi, "Long-term storage of a bit stream of solitons", Opt. Lett. **21**, 1500 – 1502 (1992).

5.7 Active Modelocking with Detuning

So far, we only considered the case of perfect synchronism between the round-trip of the pulse in the cavity and the external modulator. Technically, such perfect synchronism is not easy to achieve. One way would be to do regenerative mode locking, i.e. a part of the output signal of the modelocked laser is detected, the beatnote at the round-trip frequency is filtered out from the detector, and sent to an amplifier, which drives the modulator. This procedure enforces synchronism if the cavity length undergoes fluctuations due to acoustic vibrations and thermal expansion.

Nevertheless, it is interesting to know how sensitive the system is against detuning between the modulator and the resonator. It turns out that this is a physically and mathematically rich situation, which applies to many other phenomena occuring in externally driven systems, such as the transition from laminar to turbulent flow in hydrodynamics. This transition has puzzled physicists for more than a hundred years [1]. During the last 5 to 10 years, a scenario for the transition to turbulence has been put forward by Trefethen and others [2]. This model gives not only a quantitative description of the kind of instability that leads to a transition from laminar, i.e. highly ordered dynamics, to turbulent flow, i.e. chaotic motion, but also an intuitive physical picture why turbulence is occuring. Such a picture is the basis for many laser instabilities especially in synchronized laser systems. According to this theory, turbulence is due to strong transient growth of deviations from a stable stationary point of the system together with a nonlinear feedback mechanism. The nonlinear feedback mechanism couples part of the amplified perturbation back into the initial perturbation. Therefore, the perturbation experiences strong growth repeatedly. Once the transient growth is large enough, a slight perturbation from the stable stationary point renders the system into turbulence. Small perturbations are always present in real systems in the form of system intrinsic noise or environmental noise and, in computer simulations, due to the finite precision. The predictions of the linearized stability analysis become meaningless in such cases. The detuned actively modelocked laser is an excellent example of such a system, which in addition can be studied analytically. The detuned case has been only studied experimentally [3][4] or numerically [5] so far. Here, we consider an analytical approach. Note, that this type of instability can not be detected by a linear stability analysis which is widely used in laser theories and which we use in this course very often to prove stable pulse formation.

One has to be aware that such situations may arise, where the results of a linearized stability analysis have only very limited validity.

The equation of motion for the pulse envelope in an actively modelocked laser with detuning can be writen as

$$T_M \frac{\partial A(T,t)}{\partial T} = \left[g(T) - l + D_f \frac{\partial^2}{\partial t^2} - M\left(1 - \cos(\omega_M t)\right) + T_d \frac{\partial}{\partial t} \right] A(T,t). \tag{5.89}$$

Here, $A(T,t)$ is the pulse envelope as before. There is the time T which is coarse grained on the time scale of the resonator round-trip time T_R and the time t, which resolves the resulting pulse shape. The saturated gain is denoted by $g(T)$ and left dynamical, because we no longer assume that the gain and field dynamics reaches a steady state eventually. The curvature of the intracavity losses in the frequency domain, which limit the bandwidth of the laser, is given by D_f .and left fixed for simplicity. M is the depth of the loss modulation introduced by the modulator with angular frequency $\omega_M = 2\pi/T_M$, where T_M is the modulator period. Note that Eq.(5.89) describes the change in the pulse between one period of modulation. The detuning between resonator round-trip time and the modulator period is $T_d = T_M - T_R$.This detuning means that the pulse hits the modulator with some temporal off-set after one round-trip, which can be described by adding the term $T_d \frac{\partial}{\partial t} A$ in the master equation.The saturated gain g obeys a separate ordinary differential equation

$$\frac{\partial g(T)}{\partial T} = -\frac{g(T) - g_0}{\tau_L} - g\frac{W(T)}{P_L}. \tag{5.90}$$

As before, g_0 is the small signal gain due to the pumping, P_L the saturation power of the gain medium, τ_L the gain relaxation time and $W(T) = \int |A(T,t)|^2 \, dt$ the total field energy stored in the cavity at time T.

As before, we expect pulses with a pulse width much shorter than the round-trip time in the cavity and we assume that they still will be placed in time near the position where the modulator introduces low loss (Figure 5.15), so that we can still approximate the cosine by a parabola

$$T_M \frac{\partial A}{\partial T} = \left[g - l + D_f \frac{\partial^2}{\partial t^2} - M_s t^2 + T_d \frac{\partial}{\partial t} \right] A. \tag{5.91}$$

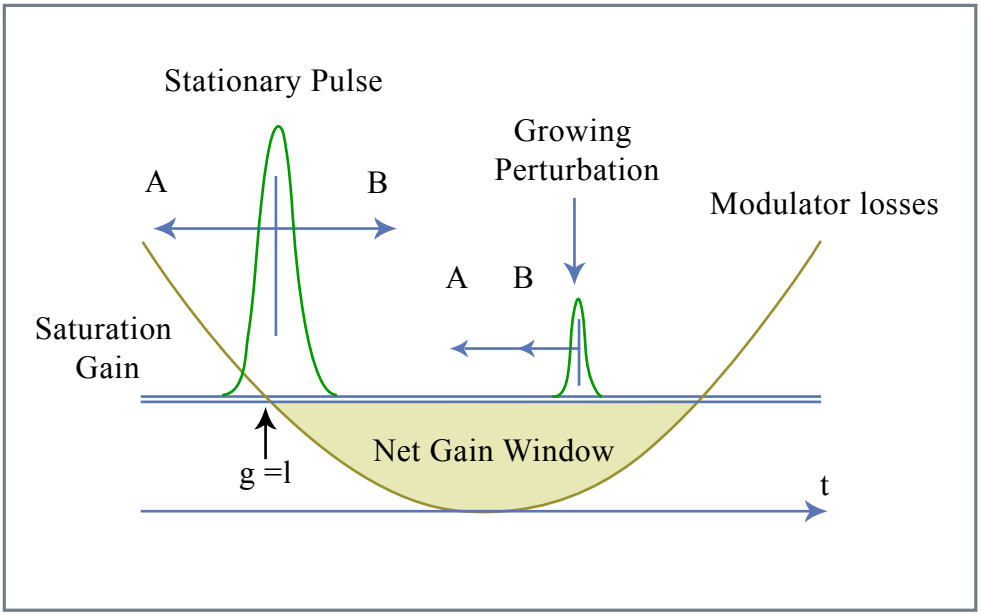

Figure 5.15: Drifting pulse dynamics in a detuned actively modelocked laser for the situation, where the modulator period is larger than the cavity round-trip time. The displacement A is caused by the mismatch between the cavity round-trip time and the modulator period. The displacement B is due to unequal losses experienced by the front and the back of the pulse in the modulator. The gain saturates to a level where a possible stationary pulse experiences no net gain or loss, which opens up a net gain window following the pulse. Perturbations within that window get amplified while drifting towards the stationary pulse.

Figure by MIT OCW.

Here, $M_s = M\omega_M^2/2$ is the curvature of the loss modulation at the point of minimum loss as before. The time t is now allowed to range from $-\infty$ to $+\infty$, since the modulator losses make sure that only during the physically allowed range $-T_R/2 \ll t \ll T_R/2$ radiation can build up.

In the case of vanishing detuning, i.e. $T_d = 0$, the differential operator on the right side of (5.91), which generates the dynamics and is usually called a evolution operator $\hat{L}$, correspondes to the Schrödinger operator of the harmonic oscillator. Therefore, it is useful to introduce the creation and annihilation operators

$$\hat{a} = \frac{1}{\sqrt{2}}\left(\frac{\tau_a \partial}{\partial t} + \frac{t}{\tau_a}\right), \quad \hat{a}^\dagger = \frac{1}{\sqrt{2}}\left(-\frac{\tau_a \partial}{\partial t} + \frac{t}{\tau_a}\right), \tag{5.92}$$

with $\tau_a = \sqrt[4]{D_f/M_s}$. The evolution operator $\hat{L}$ is then given by

$$\hat{L} = g - l - 2\sqrt{D_f M_s}\left(\hat{a}^\dagger \hat{a} + \frac{1}{2}\right) \tag{5.93}$$

and the evolution equation (5.91) can be written as

$$T_M \frac{\partial A}{\partial T} = \hat{L}A. \tag{5.94}$$

Consequently, the eigensolutions of this evolution operator are the Hermite-Gaussians, which we used already before

$$A_n(T,t) = u_n(t)e^{\lambda_n T/T_M} \tag{5.95}$$

$$u_n(t) = \sqrt{\frac{W_n}{2^n\sqrt{\pi}n!\tau_a}} H_n(t/\tau_a)e^{-\frac{t^2}{2\tau_a^2}} \tag{5.96}$$

and τ_a is the pulsewidth of the Gaussian.(see Figure 5.16a)

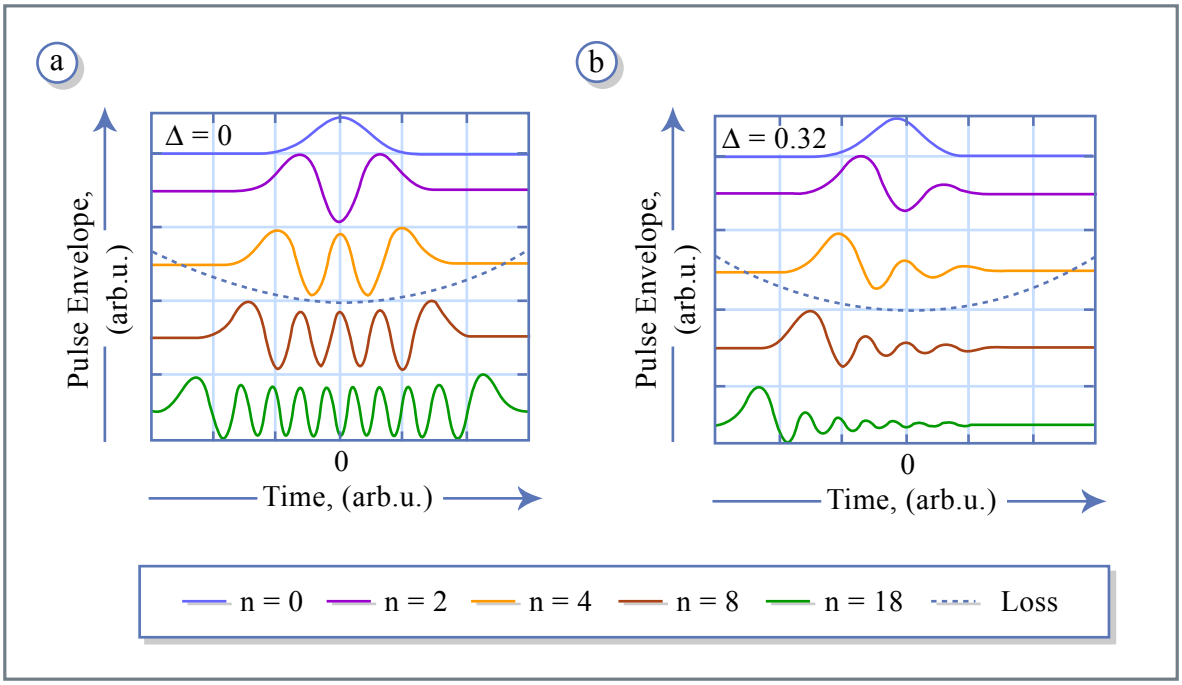

Figure 5.16: Lower order eigenmodes of the linearized system for zero detuning, $\Delta = 0$, (a) and for a detuning, $\Delta = 0.32$, in (b).

Figure by MIT OCW.

The eigenmodes are orthogonal to each other because the evolution operator is hermitian in this case.

The round-trip gain of the eigenmode $u_n(t)$ is given by its eigenvalue (or in general by the real part of the eigenvalue) which is given by $\lambda_n = g_n - l - 2\sqrt{D_f M_s}(n + 0.5)$ where $g_n = g_0\left(1 + \frac{W_n}{P_L T_R}\right)^{-1}$, with $W_n = \int |u_n(t)|^2\, dt$.

The eigenvalues prove that, for a given pulse energy, the mode with $n = 0$, which we call the ground mode, experiences the largest gain. Consequently, the ground mode will saturate the gain to a value such that $\lambda_0 = 0$ in steady state and all other modes experience net loss, $\lambda_n < 0$ for $n > 0$, as discussed before. This is a stable situation as can be shown rigorously by a linearized stability analysis [6]. Thus active modelocking with perfect synchronization produces Gaussian pulses with a $1/e$–half width of the intensity profile given by τ_a.

In the case of non zero detuning T_d, the situation becomes more complex. The evolution operator, (5.93), changes to

$$\hat{L}_D = g - l - 2\sqrt{D_f M_s}\left[\left(\hat{a}^\dagger - \Delta\right)\left(\hat{a} + \Delta\right) + (\frac{1}{2} + \Delta^2)\right] \tag{5.97}$$

with the normalized detuning

$$\Delta = \frac{1}{2\sqrt{2D_f M_s}}\frac{T_d}{\tau_a}. \tag{5.98}$$

Introducing the shifted creation and annihilation operators, $\hat{b}^\dagger = \hat{a}^\dagger + \Delta$ and $\hat{b} = \hat{a} + \Delta$, respectively, we obtain

$$\hat{L}_D = \Delta g - 2\sqrt{D_f M_s}\left(\hat{b}^\dagger\hat{b} - 2\Delta\hat{b}\right) \tag{5.99}$$

with the excess gain

$$\Delta g = g - l - 2\sqrt{D_f M_s}(\frac{1}{2} + \Delta^2) \tag{5.100}$$

due to the detuning. Note, that the resulting evolution operator is not any longer hermitian and even not normal, i.e. $\left[A, A^\dagger\right] \neq 0$, which causes the eigenmodes to become nonnormal [8]. Nevertheless, it is an easy excercise to compute the eigenvectors and eigenvalues of the new evolution operator in terms of the eigenstates of $\hat{b}^\dagger\hat{b}$, $|l\rangle$, which are the Hermite Gaussians centered around Δ. The eigenvectors $|\varphi_n\rangle$ to $\hat{L}_D$ are found by the ansatz

$$|\varphi_n\rangle = \sum_{l=0}^{n} c_l^n |l\rangle\,, \text{ with } c_{l+1}^n = \frac{n-l}{2\Delta\sqrt{l+1}}c_l^n. \tag{5.101}$$

The new eigenvalues are $\lambda_n = g_n - l - 2\sqrt{D_f M_s}(\Delta^2 + n + 0.5)$. By inspection, it is again easy to see, that the new eigenstates form a complete basis in

$L_2(I\!R)$. However, the eigenvectors are no longer orthogonal to each other. The eigensolutions as a function of time are given as a product of a Hermite Polynomial and a shifted Gaussian $u_n(t) = \langle t \,|\varphi_n\rangle \sim H_n(t/\tau_a)\, \exp\left[-\frac{(t-\sqrt{2}\Delta\tau_a)^2}{2\tau_a^2}\right]$. Again, a linearized stability analysis shows that the ground mode, i.e.$|\varphi_0\rangle$, a Gaussian, is a stable stationary solution. Surprisingly, the linearized analysis predicts stability of the ground mode for all values of the detuning in the parabolic modulation and gain approximation. This result is even independent from the dynamics of the gain, i.e. the upper state lifetime of the active medium, as long as there is enough gain to support the pulse. Only the position of the maximum of the ground mode, $\sqrt{2}\Delta \cdot \tau_a$, depends on the normalized detuning.

Figure 5.15 summarizes the results obtained so far. In the case of detuning, the center of the stationary Gaussian pulse is shifted away from the position of minimum loss of the modulator. Since the net gain and loss within one round-trip in the laser cavity has to be zero for a stationary pulse, there is a long net gain window following the pulse in the case of detuning due to the necessary excess gain. Figure 2 shows a few of the resulting lowest order eigenfunctions for the case of a normalized detuning $\Delta = 0$ in (a) and $\Delta = 0.32$ in (b). These eigenfunctions are not orthogonal as a result of the nonnormal evolution operator

5.7.1 Dynamics of the Detuned Actively Mode-locked Laser

To get insight into the dynamics of the system, we look at computer simulations for a Nd:YLF Laser with the parameters shown in Table 5.3 Figures

$E_L = 366\ \mu J$	$g_0 = 0.79$
$\tau_L = 450\ \mu s$	$M_s = 2.467 \cdot 10^{17} s^{-2}$
$\Omega_g = 1.12\ THz$	$D_g = 2 \cdot 10^{-26}\ s^2$
$T_R = 4\ ns$	$\tau_a = 17\ ps$
$l = 0.025$	$\lambda_0 = 1.047\ \mu m$
$M = 0.2$	

Table 5.3: Data used in the simulations of a Nd:YLF laser.

5.17 show the temporal evolution of the coefficient c_n,when the master equa-

tion is decomposed into Hermite Gaussians centered at t=0 according to Eq.(5.96).

$$A(T,t) = \sum_{n=0}^{\infty} c_n(T)\ u_n(t)$$

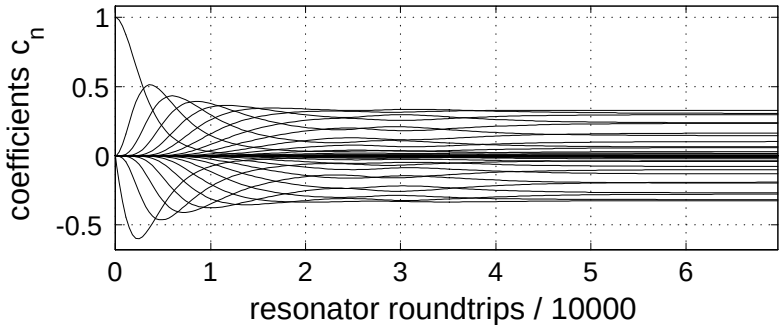

Figure 5.17: Coefficients of the envelope in a Hermite-Gaussian-Basis, as a function of resonator round-trips. The normalized detuning is $\Delta = 3.5$. The simulation starts from the steady state without detuning. The curve starting at 1 is the ground mode. To describe a shifted pulse, many modes are necessary.

Figure 5.18 and 5.19 shows the deviation from the steady state gain and the pulse envelope in the time domain for a normalized detuning of $\Delta = 3.5$.

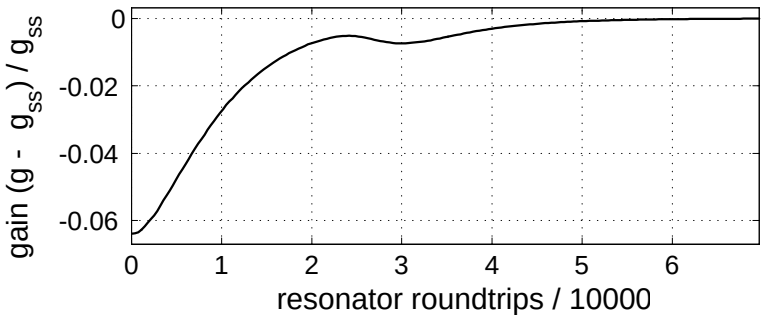

Figure 5.18: Gain as a function of the number of roundtrips. It changes to a higher level.

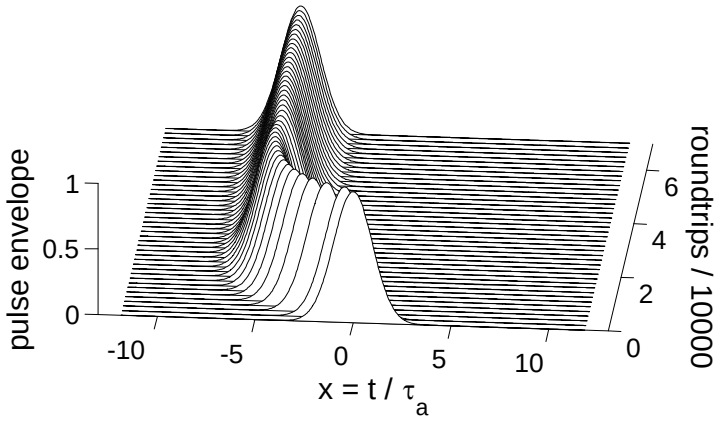

Figure 5.19: Temporal evolution of the pusle envelope. The pulse shifts slowly into the new equilibrium position at $\sqrt{2}\ \Delta = 4.9$ in agreement with the simulation.

Figures 5.20 to 5.22 show the same quantities for a slightly higher normalized detuning of $\Delta = 4$.

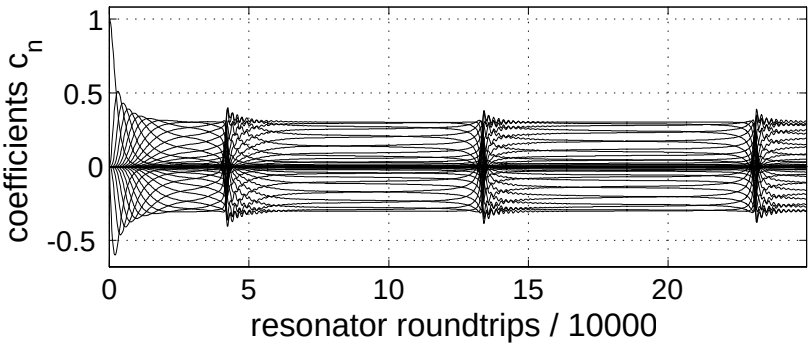

Figure 5.20: Temporal evolution of the coefficients in a Hermite-Gaussian Basis at a normalized detuning of $\Delta = 4$. Almost peridoically short interrupting events of the otherwise regular motion can be easily recognized (Intermittent Behavior). Over an extended period time between such events the laser approaches almost a steady state.

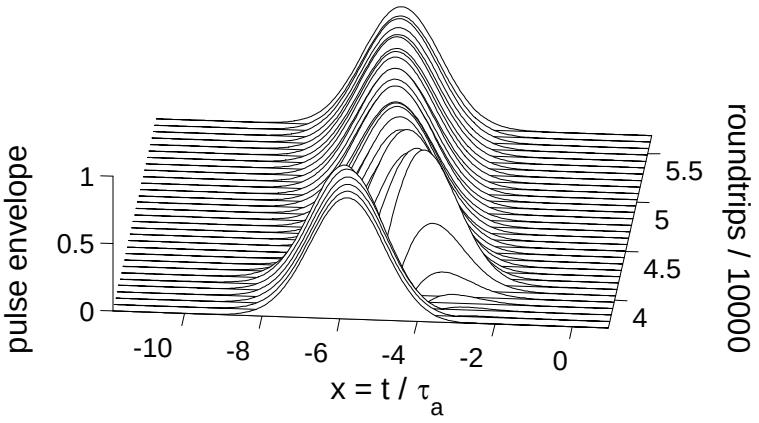

Figure 5.22: Time evolution of pulse envelope.

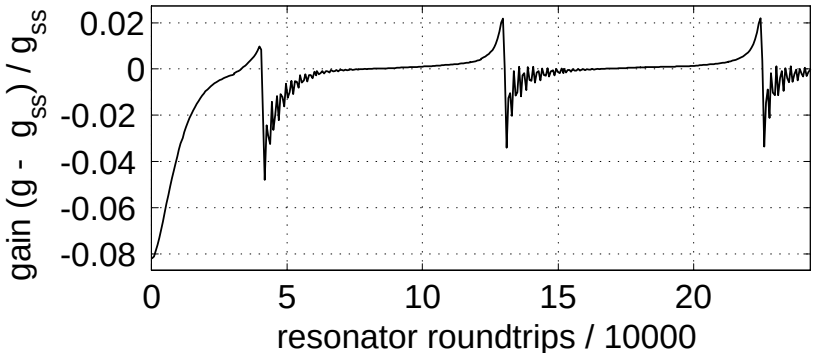

Figure 5.21: Temporal evolution of deviation from quasi steady state gain.

The pictures clearly show that the system does not approach a steady state anymore, but rather stays turbulent, i.e. the dynamics is chaotic.

5.7.2 Nonnormal Systems and Transient Gain

To get insight into the dynamics of a nonnormal time evolution, we consider the following two-dimensional nonnormal system

$$\frac{du}{dt} = Au, \quad u(0) = u_0, \quad u(t) = e^{At}u_0 \tag{5.102}$$

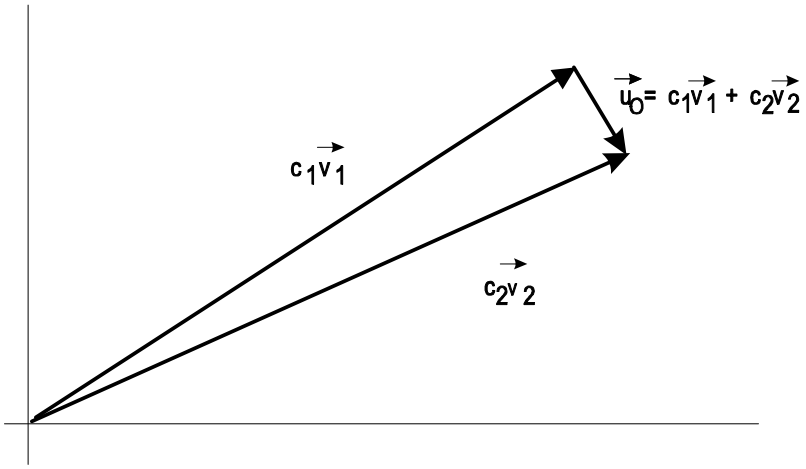

Figure 5.23: Decomposition of an initial perturbation in the eigen basis.

with

$$A = \begin{pmatrix} -\frac{1}{2} & \frac{a}{2} \\ 0 & -1 \end{pmatrix} \Rightarrow A^\dagger = \begin{pmatrix} -\frac{1}{2} & 0 \\ \frac{a}{2} & -1 \end{pmatrix}, \quad \left[A, A^\dagger\right] = \frac{a}{4}\begin{pmatrix} a & 1 \\ 1 & a \end{pmatrix} \neq 0. \tag{5.103}$$

The parameter a scales the strength of the nonnormality, similar to the detuning Δ in the case of a modelocked laser or the Reynolds number in hydrodynamics, where the linearized Navier-Stokes Equations constitute a nonnormal system.

The eigenvalues and vectors of the linear system are

$$\lambda_1 = -\frac{1}{2}, \quad v_1 = \begin{pmatrix} 1 \\ 0 \end{pmatrix}, \qquad \lambda_2 = -1, \quad v_2 = \frac{1}{\sqrt{1+a^2}}\begin{pmatrix} a \\ -1 \end{pmatrix} \tag{5.104}$$

The eigenvectors build a complete system and every initial vector can be decomposed in this basis. However, for large a, the two eigenvectors become more and more parallel, so that a decomposition of a small initial vector almost orthogonal to the basis vectors needs large components (Figure 5.23)

The solution is

$$u(t) = e^{At}u_0 = c_1 e^{-t/2}\ \overrightarrow{v}_1 + c_2\ e^{-t}\ \overrightarrow{v}_2.$$

Since the eigenvalues are negative, both contributions decay, and the system is stable. However, one eigen component decays twice as fast than

the other one. Of importance to us is the transient gain that the system is showing due to the fact of near parallel eigen vectors. Both coefficients c_1 and c_2 are large. When one of the components decays, the other one is still there and the resulting vector

$$u(t \to 2) \approx c_1 e^{-1} \overrightarrow{v}_1.$$

can be much larger then the initial perturbation during this transient phase. This is transient gain. It can become arbitrarily large for large a.

5.7.3 The Nonormal Behavior of the Detuned Laser

The nonnormality of the operator, $\left[\hat{L}_D, \hat{L}_D^\dagger\right] \sim \Delta$, increases with detuning. Figure 5.24 shows the normalized scalar products between the eigenmodes for different values of the detuning

$$C(m,n) = \left| \frac{\langle \varphi_m | \varphi_n \rangle}{\sqrt{\langle \varphi_m | \varphi_m \rangle \langle \varphi_n | \varphi_n \rangle}} \right|. \tag{5.105}$$

The eigenmodes are orthogonal for zero detuning. The orthogonality vanishes with increased detuning. The recursion relation (5.101) tells us that the overlap of the new eigenmodes with the ground mode increases for increasing detuning. This corresponds to the parallelization of the eigenmodes of the linearzed problem which leads to large transient gain, $\left\| e^{\hat{L}_D t} \right\|$, in a nonnormal situation [2]. Figure 5.24d shows the transient gain for an initial perturbation from the stationary ground mode calculated by numerical simulations of the linearized system using an expansion of the linearized system in terms of Fock states to the operator $\hat{b}$. A normalized detuning of $\Delta = 3$ already leads to transient gains for perturbations of the order of 10^6 within $20,000$ round-trips which lead to an enormous sensitivity of the system against perturbations. An analytical solution of the linearized system neglecting the gain saturation shows that the transient gain scales with the detuning according to $\exp(2\Delta^2)$. This strong super exponential growth with increasing detuning determines the dynamics completely.

Figure 5.24: Scalar products of eigenvectors as a function of the eigenvector index for the cases $\Delta = 0$ shown in (a), $\Delta = 1$ in (b) and $\Delta = 3$ in (c). (d) shows the transient gain as a funtion of time for these detunings computed and for $\Delta = 2$, from the linearized system dynamics.

Figure 5.25: Critical detuning obtained from numerical simulations as a function of the normalized pumping rate and cavity decay time divided by the upper-state lifetime. The crititcal detuning is almost independent of all laser parameters shown. The mean critical detuning is $\Delta \approx 3.65$.

Figure 5.25 shows the surface of the transition to turbulence in the parameter space of a Nd:YLF laser, i.e. critical detuning Δ, the pumping rate $r = g_0/l$ and the ratio between the cavity decay time $T_{cav} = T_R/l$ and the upper state lifetime τ_L. In this model, we did not inlcude the spontaneous emission.

The transition to turbulence always occurs at a normalized detuning of about $\Delta \approx 3.7$ which gives a transient gain $\exp(2\Delta^2) = 10^{12}$. This means that already uncertainties of the numerical integration algorithm are amplified to a perturbation as large as the stationary state itself.To prove that the system dynamics becomes really chaotic, one has to compute the Liapunov coefficient [9]. The Liapunov coefficient describes how fast the phase space trajectores separate from each other, if they start in close proximity. It is formally defined in the following way. Two trajectories $y(t)$ and $z(t)$ start in close vicinity at $t = t_0$

$$\|y(t_0) - z(t_0)\| = \varepsilon = 10^{-4}. \tag{5.106}$$

Then, the system is run for a certain time Δt and the logarithmic growth rate, i.e. Liapunov coefficient, of the distance between both trajectories is evaluated using

$$\lambda_0 = \ln\left(\frac{\|y(t_0 + \Delta t) - z(t_0 + \Delta t)\|}{\varepsilon}\right) \tag{5.107}$$

For the next iteration the trajectory $z(t)$ is rescaled along the distance between $y(t_0 + \Delta t)$ and $z(t_0 + \Delta t)$ according to

$$z(t_1) = y(t_0 + \Delta t) + \varepsilon \frac{y(t_0 + \Delta t) - z(t_0 + \Delta t)}{\|y(t_0 + \Delta t) - z(t_0 + \Delta t)\|}. \tag{5.108}$$

The new points of the trajectories $z(t_1 + \Delta t)$ and $y(t_1 + \Delta t) = y(t_0 + 2\Delta t)$ are calculated and a new estimate for the Liapunov coefficient λ_1 is calculated using Eq.(5.107) with new indices. This procedure is continued and the Liapunov coefficient is defined as the average of all the approximations over a long enough iteration, so that its changes are below a certain error bound from iteration to iteration.

$$\lambda = \frac{1}{N} \sum_{n=0}^{N} \lambda_n \tag{5.109}$$

Figure 5.26 shows the Liapunov coefficient of the Nd:YLF laser discussed above, as a function of the normlized detuning. When the Liapunov coefficient becomes positive, i.e. the system becomes exponentially sensitive to

small changes in the initial conditions, the system is called chaotic. The graph clearly indicates that the dynamics is chaotic above a critical detuning of about $\Delta_c \approx 3.7$.

Image removed due to copyright restrictions.

Please see:
Kaertner, F. X., et al. "Turbulence in Mode-locked Lasers". *Physical Review Letters* 82, no. 22 (May 1999): 4428-4431.

Figure 5.26: Liapunov coefficient over normalized detuning.

In the turbulent regime, the system does not reach a steady state, because it is nonperiodically interrupted by a new pulse created out of the net gain window, see Figure 5.15, following the pulse for positive detuning. This pulse saturates the gain and the nearly formed steady state pulse is destroyed and finally replaced by a new one. The gain saturation provides the nonlinear feedback mechanism, which strongly perturbs the system again, once a strong perturbation grows up due to the transient linear amplification mechanism.

The critical detuning becomes smaller if additional noise sources, such as the spontaneous emission noise of the laser amplifier and technical noise sources are taken into account. However, due to the super exponential growth, the critical detuning will not depend strongly on the strength of the noise sources. If the spontaneous emission noise is included in the simulation, we obtain the same shape for the critical detuning as in Fig. 5.25, however the critical detuning is lowered to about $\Delta_c \approx 2$. Note that this critical detuning is very insensitive to any other changes in the parameters of the system. Therefore, one can expect that actively mode-locked lasers without regenerative feedback run unstable at a real detuning, see (5.98) given by

$$T_d = 4\sqrt{2D_f M_s}\tau_a \tag{5.110}$$

For the above Nd:YLF laser, using the values in Table 5.3 results in a relative precision of the modulation frequency of

$$\frac{T_d}{T_R} = 1.7 \cdot 10^{-6}.$$

The derived value for the frequency stability can easily be achieved and maintained with modern microwave synthesizers. However, this requires that the cavity length of Nd:YLF laser is also stable to this limit. Note that the thermal expansion coefficient for steel is $1.6 \cdot 10^{-5}/K$.

Bibliography

[1] Lord Kelvin, Philos. Mag. **24**, 188 (1887); A. Sommerfeld, Int. Mathem. Kongr. Rom 1908, Vol. III, S. 116; W. M. F. Orr, Proc. Irish Acad. **27**, (1907).

[2] L. Trefethen, A. Trefethen, S. C. Reddy u. T. Driscol, Science **261**, 578 (1993); S. C. Reddy, D. Henningson, J. Fluid Mech. **252**, 209 (1993); Phys. Fluids **6**, 1396 (1994); S. Reddy et al., SIAM J. Appl. Math. **53**; 15 (1993); T. Gebhardt and S. Grossmann, Phys. Rev. E **50**, 3705 (1994).

[3] H. J. Eichler, Opt. Comm. **56**, 351 (1986). H. J. Eichler, I. G. Koltchanov and B. Liu, Appl. Phys. B **61**, 81 (1995).

[4] U. Morgner and F. Mitschke, Phys. Rev.A**54**, 3149 (1997).

[5] H. J. Eichler, I. G. Koltchanov and B. Liu, Appl. Phys. B **61**, 81 - 88 (1995).

[6] H. A. Haus, IEEE JQE **11**, 323 (1975).

[7] H. A. Haus, D. J. Jones, E. P. Ippen and W. S. Wong, Journal of Lightwave Technology, 14, 622 (1996).

[8] G. Bachman and L. Narici, "Functional Analysis", New York, Academic Press (1966).

[9] A. Wolf, J. B. Swift, H. L. Swinney and J. A. Vastano, Physica D **16**, 285 (1985).